

Electrochromism and photoelectrochemical performance of WO₃/Au composite film electrodes*

LIU Chunlei^{1,2}, YANG Jikai^{1,2,**}, LIU Haorui¹, and ZHAO Yiming¹

1. Chongqing Research Institute, Changchun University of Science and Technology, Chongqing 400000, China

2. School of Physics, Changchun University of Science and Technology, Changchun 130022, China

(Received 15 May 2023; Revised 21 July 2023)

©Tianjin University of Technology 2023

WO₃/Au composite film electrode was prepared by hydrothermal combined electrodeposition method. The samples were characterized by scanning electron microscope (SEM), energy dispersive spectrometer (EDS) and X-ray diffraction (XRD), and the results showed that WO₃/Au composite film was synthesized. Electrochemical and spectral measurements were carried out to obtain the electrochromic response time, reversibility, coloration efficiency (*CE*) and transmittance of the WO₃/Au composite film. The photoelectrochemical properties of the samples were characterized by measuring photocurrent and photocatalytic degradation efficiency. The results show that compared with pure WO₃ nanoblocks, WO₃/Au composite film improves the electrochromic property, photocurrent and photoelectric catalysis activity. Among them, WO₃/Au composite film prepared by depositing Au nanoparticles in 80 s showed the highest electrochromic property, photocurrent and photoelectric catalysis activity. Meanwhile, compared with direct photocatalysis (DP) and electrocatalysis (EC), the photoelectrocatalysis (PEC) activity of the composite film is the highest.

Document code: A **Article ID:** 1673-1905(2023)11-0673-8

DOI <https://doi.org/10.1007/s11801-023-3087-9>

WO₃ has been widely studied in photoelectrochemical and electrochromic fields because of its excellent photoelectrochemical activity in visible optical range, high electrochromic conversion time, reversibility and coloration efficiency (*CE*). For example, WO₃ has been regularly used in smart windows^[1], automobile rearview mirrors^[2], displays^[3], solar cells^[4] and photocatalysts^[5]. However, the disadvantages of WO₃ materials are obvious, such as low charge extraction efficiency and slow color conversion^[6,7], which will seriously affect the electrochromic properties of the WO₃. In addition, electrons and holes generated by WO₃ photoelectric catalysis are easy to recombine with each other, which will be harmful to the activity of photoelectrocatalysis (PEC)^[8,9].

In order to solve the above problems, according to research, loading Au nanoparticles (conductive materials) on the surface of WO₃ film can enhance the transfer and transmission efficiency of interface charges, thus optimizing its electrochromic properties^[10]. For example, PARK et al^[11] prepared WO₃-Au nanocomposite films by sputtering deposition method and studied its optical properties and electrochromic properties. The results show that the electrochromic performance of the WO₃-Au nanocomposite electrode has been greatly improved compared with pure WO₃. NASERI et al^[12] pre-

pared WO₃-Au composite film by sol-gel synthesis method and studied its electrochromic properties. The results show that WO₃-Au composite film has better electrochromic properties than single WO₃ film.

In addition, WO₃ loaded Au nanoparticles can not only be used as electron traps to prevent the recombination of photo-generated electron-hole pairs on the catalyst surface^[13,14], but also increase the visible light absorption of the catalyst matrix^[15,16]. For instance, ZOU et al^[17] prepared WO₃-Au composite materials by hydrothermal method and studied their photocatalytic properties. The results show that when the Au content is 2.1 wt%, the degradation rate of rhodamine B (RhB) by WO₃-Au composite materials under visible light is 6.1 times that of pure WO₃. FAUZI et al^[18] prepared Au-WO₃/rGO sensing electrodes by hydrothermal and urea-assisted deposition method and studied their gas sensing characteristics. The result shows that Au-WO₃/rGO has a good selectivity to ethanol. ZHOU et al^[19] prepared WO₃-Au/bacterial cellulose (BC) nanofiber membrane by chemical reduction and adsorption method and studied its catalytic performance. The results show that photoelectric catalytic degradation rate of tetracycline hydrochloride can reach 78.4% within 3 h, which shows higher rate than single photocatalytic rate.

* This work has been supported by the Natural Science Foundation of Chongqing City (No.CSTB2022NSCQ-MSX0751), the Education Department Project of Jilin Province (No.JJKH20220726KJ), and the Science and Technology Department Project of Jilin Province (No.20200201077JC).

** E-mail: jikaiyang0625@163.com

Unfortunately, as far as we know, there are few studies on the photoelectric catalysis of WO_3/Au composite film photoanodes, and there is almost no related research on both the photoelectrochemical properties and electrochromic properties of WO_3/Au composite film. In addition, WO_3 film prepared by hydrothermal method has excellent stability, high crystallinity, high purity and large specific surface area^[20,21], which can solve the limitations of powder samples in photoelectrochemical applications. Meanwhile, loading metal nanoparticles on WO_3 by electrodeposition is affluent to operate^[22], low in cost^[23] and good in particle uniformity^[24].

Consequently, WO_3 nanoblocks were synthesized on fluorine-doped tin oxide (FTO) substrate by hydrothermal method. The WO_3/Au composite film electrodes (WO_3/Au -40 s, WO_3/Au -80 s, WO_3/Au -120 s) were obtained by loading different amounts of Au nanoparticles (40 s, 80 s, 120 s) on WO_3 nanoblocks. Then WO_3 nanoblocks and WO_3/Au composite film were characterized systematically. The electrochromic properties of WO_3 nanoblocks and WO_3/Au composite film were evaluated by measuring response time, reversibility and *CE*. Then, under the irradiation of visible light, the photoelectrochemical properties of WO_3 nanoblocks and WO_3/Au composite film were characterized by photocurrent and PEC measurement. The PEC, direct photocatalysis (DP) and electrocatalysis (EC) experiments were carried out on WO_3/Au composite film, and the experimental results were analyzed theoretically to verify the advantages of PEC process.

Materials included ethanol, NaOH, 97 wt% H_2SO_4 , 37 wt% HCl (Beijing Chemical works, China), $\text{Na}_2\text{WO}_4 \cdot 2\text{H}_2\text{O}$, $(\text{NH}_4)_2\text{C}_2\text{O}_4 \cdot \text{H}_2\text{O}$ (Tianjin Guangfu Technology Development Co., Ltd., China), HAuCl_4 (Sinopharm Group Chemical Reagent Co., Ltd., China), Na_2SO_4 , methylene blue (MB, Xilong Chemical Co., Ltd., China), LiClO_4 , propylene carbonate (PC) (Shanghai Maclean Biochemical Technology Co., Ltd., China), N_2 (Changchun Juyang Gas Co., Ltd., China), and FTO substrates (F: SnO_2 , $8 \Omega \cdot \text{sq}^{-1}$, transparency 80%; Pilkington, United States). Deionized water is homemade in the laboratory. All reagents are analytical grade.

Scanning electron microscope (SEM) was used to analyze the surface morphology of the sample. The crystal structure of the sample was characterized by X-ray diffraction (XRD, Rigaku D/MAX 2550 V/PC, Rigaku Corporation, Japan), and photoelectrochemistry and electrochromic tests were enforced on the same workstation (LK98C, Lanlike Instrument Corp, Tianjin, China). A 300 W xenon lamp with a 420 nm cut-off filter was served as the light source (50 W, PLS-SXE300, Perfect light Instrument Corp, Beijing, China). The ultraviolet-visible (UV-Vis) diffuse reflectance spectrum (DRS) of the sample was measured by UV-Vis-NIR spectrophotometer (Cary 5000, Agilent Technologies Inc.). The change of dye concentration was analyzed by UV-Vis spectrophotometer (TU-1810, Beijing Purkinje

General Instrument Co., Ltd., China).

Firstly, the FTO substrate is placed in the mixed solution of ethanol, acetone and NaOH for ultrasonic treatment 15 min, and then continuously cleaned with deionized water for 10 min. The FTO samples were taken out and dried in N_2 gas flow at room temperature. The preparation process of WO_3 is based on hydrothermal method. Firstly, 2.31 g $\text{Na}_2\text{WO}_4 \cdot 2\text{H}_2\text{O}$ is dissolved in 70 mL deionized water, after that 50 mL of 3.0 M HCl is put in it, which is stirred continuously until the mixed solution turns pale yellow. Then, 2.0 g $(\text{NH}_4)_2\text{C}_2\text{O}_4$ is added and stirred until the solution is transparent. The solution (3 mL) prepared by the above method is transferred to a 25 mL polytetrafluoroethylene (PTFE) liner and placed in a stainless-steel autoclave. Finally, the FTO substrate is placed at an angle against the lining wall, with the conductive surface facing down. The hydrothermal reaction was carried out at 150 °C for 4 h. After the hydrothermal reaction, the sample was drawn out, cleaned with deionized water, and then dried at room temperature in N_2 stream. Finally, WO_3 samples were dried at 60 °C for 30 min, and then annealed at 450 °C in air for 1 h.

The preparation process of Au nanoparticles is based on electrodeposition. First, WO_3 sample was soaked in 1 mM $\text{AuCl}_3 \cdot \text{HCl} \cdot 4\text{H}_2\text{O}$ solution (including 0.5 M H_2SO_4) and used as working electrode. Pt foil is used as counter electrode, and Ag/AgCl electrode is used as reference electrode. The three-electrode battery is connected to LK98C electrochemical workstation. For Au nanoparticles, the deposition potential is -0.6 V (relative to Ag/AgCl) and the deposition time is 40 s, 80 s and 120 s, respectively. The WO_3/Au samples were cleaned with deionized water and then annealed in air at 300 °C for 30 min.

Electrochromic measurement was carried out on LK98C workstation. Three-electrode method was used, with WO_3/Au composite film as working electrode, Pt foil as counter electrode, and Ag/AgCl electrode as reference, which was carried out in 100 mL 1 M LiClO_4/PC solution. The potential was set between -1 V and +1 V, and the cyclic voltammetry (CV) test was performed at a scanning rate of 50 mV/s. The chronoamperometry (CA) and chronocoulometry (CC) were carried out for 50 s at -1 V and +1 V potentials, respectively. Then the response time, reversibility and *CE* of all samples can be gained. The spectrum was measured by UV-Vis spectrophotometer in the range from 400 nm to 800 nm.

Photoelectrochemical measurement is also carried out on LK98C workstation, with WO_3/Au composite film as working electrode, Pt foil as counter electrode, Ag/AgCl electrode as reference electrode and 0.01 M Na_2SO_4 solution as electrolyte. The light source for simulating visible light irradiation is a 300 W Xe lamp with a 420 nm cut off filter. Irradiating the electrode from the front, the area exposed to light is 2.25 cm^2 , and the incident light intensity on the electrode surface is 50 mW/cm^2 . Before

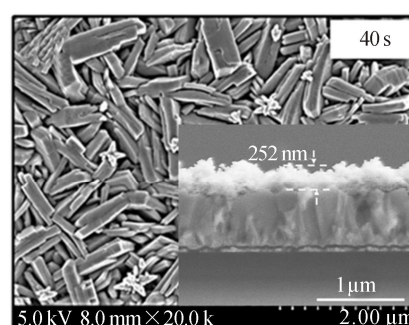
the experiment, in order to make the dye molecule disperse well, three electrodes were immersed in the dye for 20 min, and the absorption/desorption balance between the organic molecules and the photoanode surface was established. PEC activity of WO_3/Au composite film photoanode was appraised by examining the degradation of MB solution (90 mL, $\text{MB}=6 \text{ mg}\cdot\text{L}^{-1}$, $\text{Na}_2\text{SO}_4=0.01 \text{ M}$) under simulated visible light irradiation and 1.5 V bias voltage. Meanwhile, direct photocatalytic performance of WO_3/Au composite film photoanode under simulated visible light irradiation was evaluated. Given the interval of 20 min, the detection wavelength is 665 nm, and the concentration change of MB dye is tested by UV-Vis spectrophotometer (TU-1810). The measurement of electrochemical impedance spectroscopy (EIS) was carried out in Na_2SO_4 solution, with the frequency scanning range of 1—100 000 Hz, the bias voltage of 0.01 V (vs. Ag/AgCl) and the amplitude of AC voltage of 5 mV.

In Fig.1(a—c), the microstructures of WO_3 nanoblocks, $\text{WO}_3/\text{Au-40 s}$, $\text{WO}_3/\text{Au-80 s}$ and $\text{WO}_3/\text{Au-120 s}$ were observed by SEM. The prepared pure WO_3 film is primarily made of plenty of brick-like structures. It can be seen that the thickness of $\text{WO}_3/\text{Au-40 s}$, $\text{WO}_3/\text{Au-80 s}$ and $\text{WO}_3/\text{Au-120 s}$ are 252 nm, 257 nm and 261 nm, respectively. Because all WO_3/Au composite films are based on WO_3 thin films, there is no obvious change in morphology compared with pure WO_3 nanoblocks. In $\text{WO}_3/\text{Au-40 s}$, $\text{WO}_3/\text{Au-80 s}$ and $\text{WO}_3/\text{Au-120 s}$, it can be clearly observed that Au nanoparticles are attached to the surface of WO_3 nanoblocks, and the amount of Au nanoparticles increases with the increase of electrodeposition time. However, the distribution of Au nanoparticles on the surface of WO_3/Au composite film is not uniform, and some Au nanoparticles are clustered. The results showed that WO_3/Au composite film was synthesized. The energy dispersive spectrometer (EDS) energy spectrum of $\text{WO}_3/\text{Au-80 s}$ is analyzed in Fig.1(d). From the figure, Au, C, W and O elements can be observed, but no other impurity elements are observed, which further proves that WO_3/Au composite film has been synthesized.

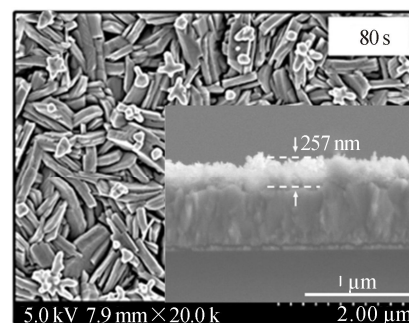
Then, the crystal structure of the samples was characterized by XRD. Fig.1(e) shows the XRD patterns of WO_3 and $\text{WO}_3/\text{Au-80 s}$ composite films. It can be observed from the figure that there are obvious diffraction peaks 2θ (Bragg angle) at 23.1° , 23.6° , 24.3° , 33.6° , 38.6° , 43.8° , 50.1° and 55.1° . All the peaks can be regarded as cubic WO_3 crystal structure (JCPDS No. 41-0905). In addition, the diffraction peak of FTO (JCPDS No.46-1088) was also observed. Unfortunately, the diffraction peak of Au was not observed in the XRD pattern of $\text{WO}_3/\text{Au-80 s}$ composite film. We think this can be attributed to the fact that Au is lower than the detection limit of XRD.

The UV-Vis absorption spectra of WO_3 nanoblocks and $\text{WO}_3/\text{Au-80 s}$ composite film are calculated from their diffuse reflectance test data and shown in Fig.2.

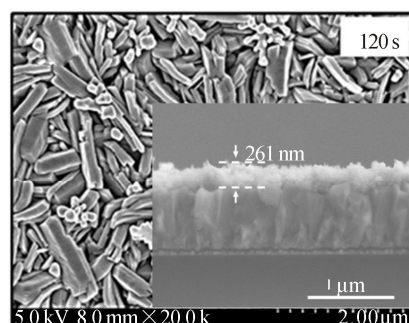
$\text{WO}_3/\text{Au-80 s}$ composite film shows similar absorption spectrum to WO_3 nanoblocks. However, compared with pure WO_3 nanoblocks, the visible light absorption of WO_3/Au composite film is obviously enhanced, and the absorption curve exhibits obvious red-shift, which is consistent with the research of MINGGU *et al.*^[25]. This significantly enhances the absorption range of the spectrum and improves the utilization rate of solar energy. This can be attributed to the local surface plasmon resonance (LSPR) effect of Au nanoparticles^[26,27].



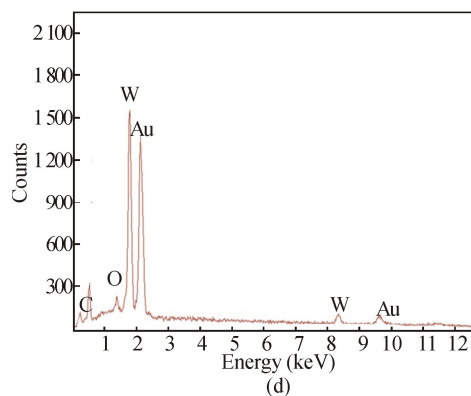
(a)



(b)



(c)



(d)

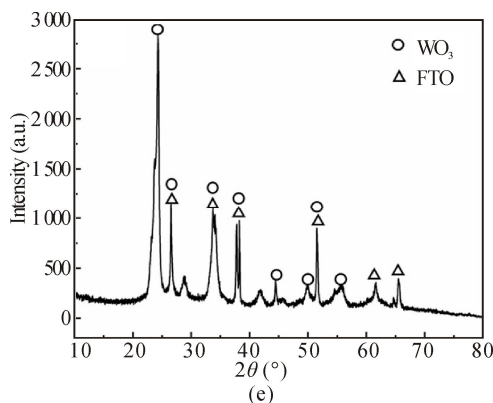


Fig.1 Structure and characterization of WO₃ nanoblocks and WO₃/Au composite films: (a—c) Surface and cross section SEM images of WO₃/Au-40 s, WO₃/Au-80 s and WO₃/Au-120 s; (d) EDS of WO₃/Au-80 s; (e) XRD patterns of WO₃ nanoblocks and WO₃/Au-80 s

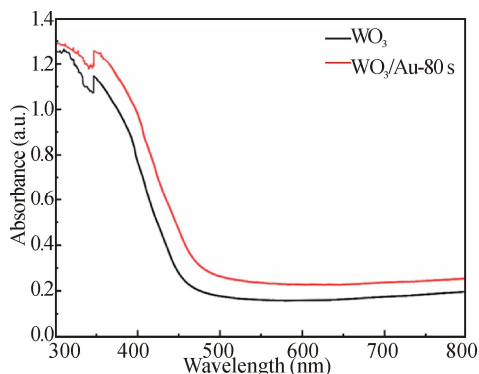


Fig.2 UV-Vis absorption spectra of WO₃ nanoblocks and WO₃/Au-80 s

The electrochromic performances of WO₃ nanoblocks and WO₃/Au composite films are characterized by CV, CC, CA and spectral measurement. Fig.3(a) shows the CV curves of WO₃ nanoblocks and WO₃/Au composite films. The scanning rate was set at 50 mV/s, and the films were scanned with a potential between -1 V and +1 V. It can be clearly seen that all samples have an obvious oxidation peak, but no reduction peak was observed. Besides, the closed area of WO₃/Au composite film is larger than pure WO₃ film and the closed area of WO₃/Au-80 s is the largest. In addition, the closed area of CV curve reflects the capacity of Li⁺ ions, which means that the deposition of Au improves the Li⁺ ions capacity of WO₃ films. Fig.3(b) shows the CC curves of WO₃ nanoblocks, WO₃/Au-40 s, WO₃/Au-80 s and WO₃/Au-120 s composite films at 1.0 V for 50 s. According to the values of inserting charge Q_i and extracting charge Q_{di} , the reversibility of all samples was reckoned by using the following relationship: $\text{reversibility} = Q_{di}/Q_i$ ^[28]. The reversibility values of WO₃ nanoblocks, WO₃/Au-40 s, WO₃/Au-80 s and WO₃/Au-120 s composite films were given in Tab.1. The sequence of electrochromic reversibility is WO₃/Au-80 s > WO₃/Au-40 s >

WO₃/Au-120 s > WO₃ nanoblocks, which indicates that Au deposition also improves the electrochromic reversibility of WO₃. The electrochromic reversibility of WO₃/Au-80 s is 87.41%, which is 1.36 times that of WO₃ samples. The response time is essential to electrochromic materials under alternating electric potential. The response time of WO₃ nanoblocks, WO₃/Au-40 s, WO₃/Au-80 s and WO₃/Au-120 s composite films was studied through CA measurement. Fig.3(c) exhibits the measurement of WO₃ nanoblocks and WO₃/Au composite films under coloring and bleaching state by CA method. The response time was obtained by applying a potential between -1.0 V and +1 V in turn for 50 s at wavelength of 700 nm, and it was used to study the electrochromic properties. Response time refers to the time it takes for the transmittance of the sample to reach 90% from bleaching to coloring^[29]. The response time of WO₃ nanoblocks and WO₃/Au composite films is recited in Tab.1, where t_b and t_c are the response time of sample coloring and bleaching. According to the data of Tab.1, WO₃/Au-80 s composite film shows the shortest response time.

CE is one of the important parameters to evaluate the electrochromic properties of electrodes. The value of CE is calculated by using the following equation^[30]

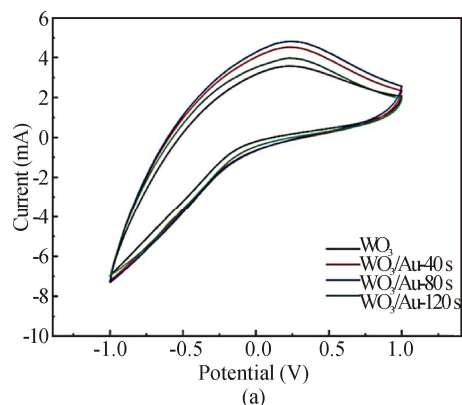
$$CE = \Delta OD / Q, \tag{1}$$

where Q is the charge density and ΔOD is the optical density, which can be gained by the transmission spectra recorded in the bleaching/coloring state of WO₃ nanoblocks and WO₃/Au composite films as shown in Fig.4. ΔOD of all samples at 700 nm are calculated by^[31]

$$\Delta OD = \log(T_b / T_c), \tag{2}$$

where T_b and T_c are the transmittance of samples in their bleaching and coloring states, respectively. The parameters were given in Tab.1. In addition, the ΔOD values of WO₃ nanoblocks, WO₃/Au-40 s, WO₃/Au-80 s and WO₃/Au-120 s were also obtained and given in Tab.1. Therefore, the CE values of WO₃ nanoblocks and WO₃/Au composite films are obtained by Eq.(1), as shown in Tab.1.

The result of ΔOD and CE is WO₃/Au-80 s > WO₃/Au-40 s > WO₃/Au-120 s > WO₃ nanoblocks, indicating that Au deposition improves the CE and optical density of



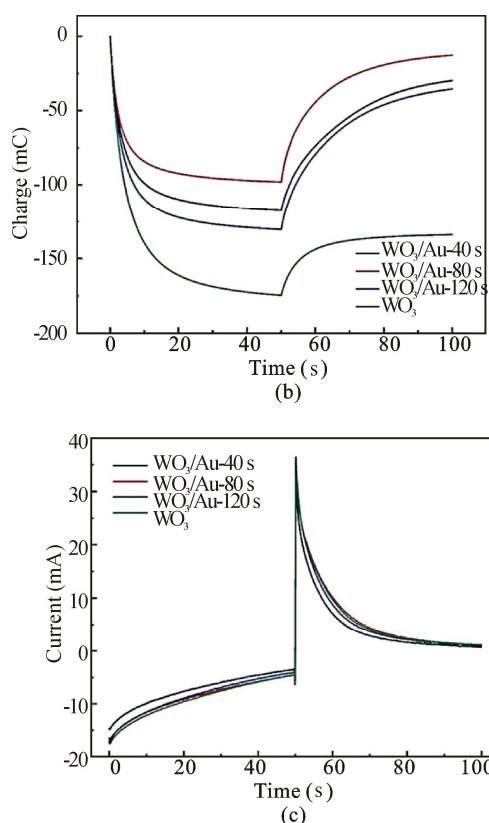


Fig.3 Electrochromic properties of WO_3 nanoblocks and WO_3/Au composite films: (a) CV curves; (b) CC curves; (c) CA curves

Tab.1 Electrochromic property parameters of WO_3 nanoblocks and WO_3/Au composite films

Parameter	$\text{WO}_3/\text{Au-40 s}$	$\text{WO}_3/\text{Au-80 s}$	$\text{WO}_3/\text{Au-120 s}$	WO_3
Reversibility (%)	74.65	87.41	72.79	64.04
t_c (s)	46.18	41.45	42.63	42.91
t_b (s)	29.19	23.14	31.62	30.94
T_b (%)	56.04	55.05	36.25	80.64
T_c (%)	31.45	16.76	13.03	57.84
ΔOD	0.25	0.32	0.24	0.14
CE (cm^2C^{-1})	70.42	88.89	66.1	38.56

WO_3 , and the CE of $\text{WO}_3/\text{Au-80 s}$ is the best, which is 2.3 times that of pure WO_3 . Through the above research, it is found that the electrochromic property of WO_3/Au composite films is indeed enhanced. The reasons for the enhancement can be attributed to the following aspects: on the one hand, Au was deposited on WO_3 to form composite film, which increased the conductivity and enhanced the insertion/extraction of electrons and ions. On the other hand, the optical absorption band gap has different effects on the electrochromic properties. The $\text{WO}_3/\text{Au-80 s}$ composite film with the best electrochromic performance is taken as an example. $\text{WO}_3/\text{Au-80 s}$ composite film has a lower optical absorption band gap, which promotes the generation of quantities of free electrons. Eventually, the free electrons will occupy the t_{2g} band of WO_3 . Therefore, the electrochromic property of

the composite film is improved, and the color contrast is also increased^[32]. Finally, due to the difference of work function, a metal-semiconductor Schottky barrier is formed at the WO_3/Au interface, which can act as a trap to capture electrons. Consequently, the efficiency of charge transfer and transmission are enhanced, and the electrochromic property is also improved. However, excessive deposition of Au nanoparticles will damage the electrochromic properties of the composite film, such as hindering the transfer of charge, which will eventually lead to the reduction of cyclic voltammogram area, reversibility and CE .

In order to study the photoelectrochemical properties of WO_3/Au composite films, the photocurrent and photoelectrocatalytic activity of all samples were measured. Fig.5(a) shows $I-V$ curves of WO_3 nanoblocks and WO_3/Au composite films under visible light irradiation. The results show that the photocurrent of all samples generally increases with the increase of bias voltage, and the dark current can be neglected. At the same time, the sequence of photocurrent is $\text{WO}_3/\text{Au-80 s} > \text{WO}_3/\text{Au-120 s} > \text{WO}_3/\text{Au-40 s} > \text{WO}_3$ nanoblocks. The photocurrent of WO_3/Au composite film is higher than that of WO_3 nanoblocks, especially $\text{WO}_3/\text{Au-80 s}$. The PEC measurement was carried out under the bias voltage of 1.5 V, where the photocurrent difference of the sample was the most obvious. Fig.5(b) shows the photoelectrocatalytic degradation efficiency (C/C_0) of MB degraded by WO_3 nanoblocks and WO_3/Au composite films, where C represents the MB concentration at different catalytic degradation times, and C_0 represents the initial MB concentration. The result of photoelectric catalysis is $\text{WO}_3/\text{Au-80 s} > \text{WO}_3/\text{Au-120 s} > \text{WO}_3/\text{Au-40 s} > \text{WO}_3$ nanoblocks. The degradation rate of WO_3/Au composite film is higher than that of WO_3 nanoblocks, and $\text{WO}_3/\text{Au-80 s}$ shows the highest photoelectric catalysis activity, which is mutually confirmed by the photocurrent measurement results. To reflect the superiority of PEC, $\text{WO}_3/\text{Au-80 s}$ composite film was selected and measured by photoelectric catalysis, DP and electrocatalysis, and the results were shown in Fig.5(c). DP was carried out under visible light irradiation. On the contrary, electrocatalysis was carried out under dark conditions by applying a bias voltage of 1.5 V (vs. Ag/AgCl). In Fig.5(c), the order of observed activities is $\text{PEC} > \text{DP} > \text{EC}$. In DP process, WO_3/Au composite film produced electron-hole pairs under simulated visible light irradiation. The electrons of WO_3 interface are transported to Au nanoparticles, at this moment a large number of holes remain on WO_3 surface, resulting in redox reaction. At the same time, electrons and holes may recombine. When the recombination rate is too high, the catalytic efficiency will be seriously affected. In EC process, the WO_3/Au composite film photoanode generates electron-hole pairs at a 1.5 V (vs. Ag/AgCl) bias potential. After that the electrons and holes are separated. However, the creation efficiency of

electron-hole pairs is still low, which results in low catalytic efficiency. In the PEC process, the electron-hole pairs are created under simulated visible light irradiation. Meanwhile, the electron-hole pairs have been further created and electrons were separated from holes under the external bias potential 1.5 V (vs. Ag/AgCl). The results show that the creation and separation of electrons and holes can be effectively promoted in the PEC process. EIS analysis was used to study the charge transfer process. As shown in Fig.5(d), the EIS Nyquist diagram of WO₃ nanoblocks and WO₃/Au-80 s was studied. The arc radius in EIS curve can reflect the electron transfer resistance inside the sample electrode. The larger the arc radius, the greater the charge transfer resistance between the electrode and the electrolyte, and the lower the electron transfer efficiency inside the sample electrode^[33].

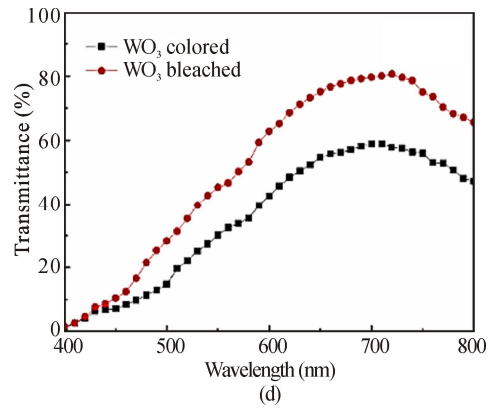
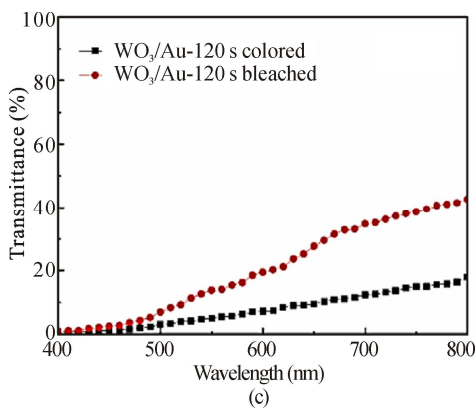
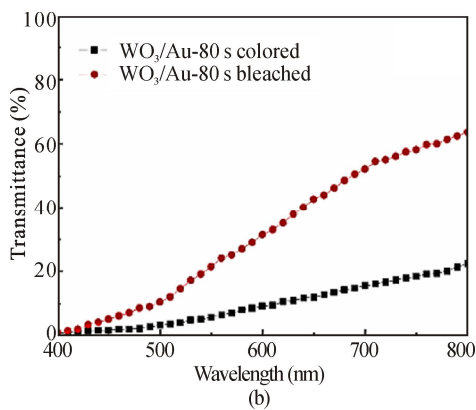
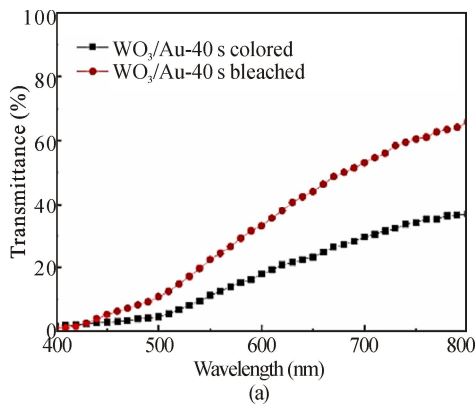
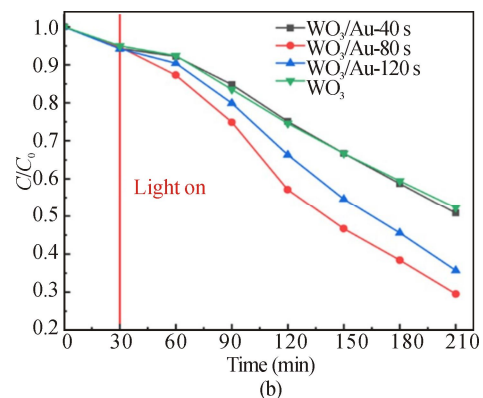
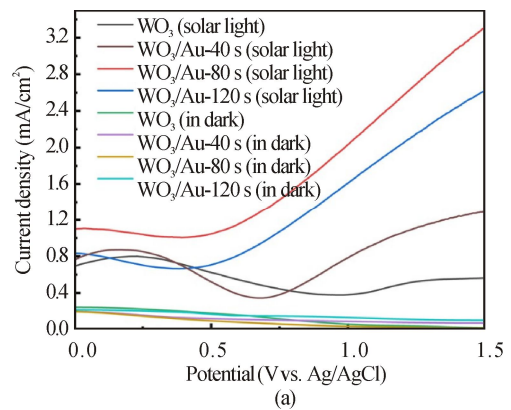


Fig.4 Transmittance spectra of WO₃ and WO₃/Au composite films at the bleached/colored state (700 nm): (a) WO₃/Au-40 s; (b) WO₃/Au-80 s; (c) WO₃/Au-120 s; (d) WO₃ nanoblocks



The arc radius of WO₃ nanoblocks is larger than WO₃/Au-80 s, which indicates that the loading of Au nanoparticles greatly promotes the charge transfer from WO₃ to Au, which is due to the effective capture of electrons by Au^[14,16]. EIS analysis results once again confirmed that WO₃/Au composite film photoanode had higher photocurrent and PEC activity than pure WO₃.

To sum up, WO₃/Au-80 s composite film shows the highest photocurrent and PEC activity, thus confirming the excellent photoelectrochemical performance of the samples. This can be attributed to the following two aspects. On the one hand, according to the results of absorption spectrum in Fig.2, depositing Au on WO₃ can



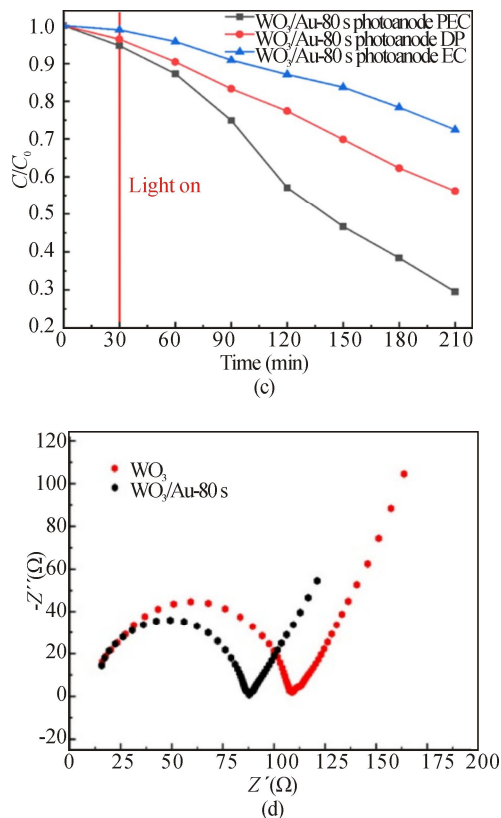


Fig.5 (a) *I-V* curves of WO₃ nanoblocks and WO₃/Au composite films; (b) PEC activity of WO₃ nanoblocks and WO₃/Au composite films; (c) Photoelectrocatalytic cycle tests of WO₃/Au-80 s; (d) Nyquist plots of WO₃ nanoblocks and WO₃/Au-80 s

indeed increase the absorption range of visible light, which is beneficial to the generation of electrons and holes. Therefore, WO₃/Au composite film photoanode has higher photocurrent and PEC activity than pure WO₃. On the other hand, according to the results shown in Fig.5(d), the metal-semiconductor Schottky barrier at the WO₃/Au interface can be used as a trap to capture electrons, which promotes the separation of electron-hole pairs in WO₃^[14,16]. Electron transfers from WO₃/Au interface to Au, leaving more holes on WO₃ surface. Therefore, the WO₃/Au composite film shows larger photocurrent and higher PEC activity than pure WO₃. However, if Au nanoparticles are loaded excessively, they will occupy the surface active sites of WO₃, which is unfavorable to photocurrent and PEC activity.

In this paper, WO₃/Au composite film was prepared by hydrothermal method combined with electrodeposition. WO₃/Au composite film has a larger visible light absorption range than WO₃ nanoblocks. Meanwhile, the charge transfer efficiency of WO₃/Au composite film is higher than that of pure WO₃ film. WO₃/Au-80 s composite film has the large photocurrent, the best electrochromic and photoelectric catalysis properties. Besides, compared with DP and EC, the PEC activity of the composite film is the highest. In this paper, it shows that WO₃/Au composite film has a broad development space and market in

degradation of organic pollutants and electrochromic applications, and it also lays a foundation for the research of photoelectric properties of noble metal/semiconductor systems.

Ethics declarations

Conflicts of interest

The authors declare no conflict of interest.

References

- [1] CLAES G, GRANQVIS T. Electrochromics for smart windows: oxide-based thin films and devices[J]. Thin solid films: an international journal on the science and technology of thin and thick films, 2014, 564: 1-38.
- [2] SONG Y L, ZHANG Q Y, YAO A H. Template-free electrodeposition and electrochromic performance of porous WO₃·2H₂O thin film[J]. Chinese journal of inorganic chemistry, 2023, 39(01): 127-134.
- [3] WANG M, FANG G, YUAN L, et al. High optical switching speed and flexible electrochromic display based on WO₃ nanoparticles with ZnO nanorod arrays supported electrode[J]. Nanotechnology, 2009, 20(18): 185304.
- [4] WANG Y Q, NIE L H, WU N, et al. Preparation of WO₃ nanoarray by hydrothermal method and its application in perovskite solar cells[J]. Journal of the Chinese ceramic society, 2018, 46(05): 649-656.
- [5] KERAN W, LUO L, WANG C, et al. Photocatalytic methane activation by dual reaction sites commodified WO₃[J]. Chinese journal of catalysis, 2023, 46(03): 103-112.
- [6] WEN R T, GRANQVIST C G, NIKLASSON G A. Eliminating degradation and uncovering ion-trapping dynamics in electrochromic WO₃ thin films[J]. Nature materials, 2015, 14: 996-1001.
- [7] WEN R T, ARVIZU M A, MORALES-LUNA M, et al. Ion trapping and detrapping in amorphous tungsten oxide thin films observed by real-time electro-optical monitoring[J]. Chemistry of materials, 2016, 28: 4670-4676.
- [8] YA J, YUE X P, ZHANG A M. Preparation of pseudo-single crystal WO₃ nanosheets and their photocatalytic performance[J]. China environmental science, 2021, 41(04): 1615-1623.
- [9] KARUPPASAMY K M, SUBRAHMANYAM A. The electrochromic and photocatalytic properties of electron beam evaporated vanadium-doped tungsten oxide thin films[J]. Solar energy materials and solar cells, 2008, 92(11): 1322-1326.
- [10] RAHMANZADE K A, NIKFARJAM A, AMERI M, et al. Improving electrochromic properties of WO₃ thin film with Au nanoparticle additive[J]. International journal of engineering, 2015, 28(8): 1169-1174.
- [11] PARK K W. Electrochromic properties of Au-WO₃ nanocomposite thin-film electrode[J]. Electrochimica acta, 2005, 50(24): 4690-4693.

- [12] NASERI N, AZIMIRAD R, AKHAVAN O, et al. Improving the electrochromic properties of sol-gel WO_3 films by doping Au nanocrystals[J]. *Thin solid films*, 2010, 518(8): 2250-2257.
- [13] PENNINGTON A M, PITMAN C L, DESARIO P A, et al. Photocatalytic CO oxidation over nanoparticulate Au-modified TiO_2 aerogels: the importance of size and intimacy[J]. *ACS catalysis*, 2020, 10(24) : 14834-14846.
- [14] WANG Z L, LAI L W, WANG Y C, et al. Preparation and enhanced photoelectrocatalytic properties of a three-dimensional TiO_2 Au porous structure fabricated using super aligned carbon nanotube films[J]. *International journal of hydrogen energy*, 2020, 45(56) : 31963-31975.
- [15] NG K H, MINGGU L J, JAAFAR N A, et al. Enhanced plasmonic photoelectrochemical response of Au sandwiched WO_3 photoanodes[J]. *Solar energy materials and solar cells*, 2017, 172: 361-367.
- [16] XU F, YAO Y, BAI D, et al. A significant cathodic shift in the onset potential and enhanced photoelectrochemical water splitting using Au nanoparticles decorated WO_3 nanorod array[J]. *Journal of colloid and interface science*, 2015, 458: 194-199.
- [17] ZOU J W, LI Z D, KANG H S. Strong visible light absorption and abundant hotspots in Au-decorated WO_3 nanobricks for efficient SERS and photocatalysis[J]. *ACS omega*, 2021, 6(42): 28347-28355.
- [18] FAUZI A S A, HAMIDAH N L, KITAMURA S, et al. Electrochemical detection of ethanol in air using graphene oxide nanosheets combined with Au- WO_3 [J]. *Sensors (Basel)*, 2022, 22(9): 3194.
- [19] ZHOU T, WANG D B, ZHAO L, et al. Preparation of bacterial cellulose/Au film loaded with tungsten trioxide and its catalytic performance[J]. *Journal of textile research*, 2023, 44(04): 16-23.
- [20] DU J, YANG M D, WU Y L, et al. The effects of solvent and microwave on the preparation of magnesium oxide precursor[J]. *Crystal research & technology*, 2015, 49(12): 959-964.
- [21] YAN C, MA Q, JIA H, et al. Hydrothermal synthesis of ZnS microspheres with highly effective photocatalytic and antibacterial properties[J]. *Journal of materials science : materials in electronics*, 2016, 27(10) : 10237-10243.
- [22] OZDAL T, TAKTAKOGLU R, OZDAMAR H, et al. Crystallinity improvement of ZnO nanorods by optimization of low-cost electrodeposition technique[J]. *Thin solid films*, 2015, 592(OCT.1PT.A): 143-149.
- [23] SUN M, ZANGARI G, SHAMSUZZOHA M, et al. Electrodeposition of highly uniform magnetic nanoparticle arrays in ordered alumite[J]. *Applied physics letters*, 2001, 78(19): 2964-2966.
- [24] TAO F F, GUAN M Y, JIANG Y, et al. An easy way to construct an ordered array of nickel nanotubes: the triblock-copolymer-assisted hard-template method[J]. *Advanced materials*, 2010, 18(16): 2161-2164.
- [25] MINGGU L J, JAAFAR N A, NG K H, et al. Electrodeposited WO_3/Au photoanodes for photoelectrochemical reactions[J]. *Sains malaysia*, 2020, 49(12): 3209-3217.
- [26] WANG J, JIANG L, LIU F, et al. Enhanced photoelectrochemical degradation of tetracycline hydrochloride with FeOOH and Au nanoparticles decorated WO_3 [J]. *Chemical engineering journal*, 2021, 407: 127195.
- [27] ZHANG B, WANG H, YE H. Reversible redox mechanism based synthesis of plasmonic WO_3/Au photocatalyst for selective and sensitive detection of ultra-micro Hg^{2+} [J]. *Sensors and actuators B: chemical*, 2018, 273: 1435-1441.
- [28] PATIL P S, MUJAWAR S H, INAMDAR A I, et al. Electrochromic properties of spray deposited TiO_2 doped WO_3 thin films[J]. *Applied surface science*, 2005, 250(1-4): 117-123.
- [29] YAN C, KANG W, WANG J. Stretchable and wearable electrochromic devices[J]. *ACS nano*, 2014, 8(1): 316-322.
- [30] ADHIKARI S, SWAIN R, SARKAR D, et al. Wedge-like WO_3 architectures for efficient electrochromism and photoelectrocatalytic activity towards water pollutants[J]. *Molecular catalysis*, 2017, 432: 76-87.
- [31] KARUPPASAMY A. Electrochromism and photocatalysis in dendrite structured Ti: WO_3 thin films grown by sputtering[J]. *Applied surface science*, 2015, 359(DEC.30): 841-846.
- [32] ZHANG G G, LU K K, ZHANG X C, et al. Effects of annealing temperature on optical band gap of sol-gel tungsten trioxide films[J]. *Micromachines*, 2018, 9: 3771-3779.
- [33] MA B, YU N, XIN S, et al. Photoelectrocatalytic degradation of p-chloronitrobenzene by g- $\text{C}_3\text{N}_4/\text{TiO}_2$ nanotube arrays photoelectrodes under visible light irradiation[J]. *Chemosphere*, 2021, 267: 129242.